Hindawi
Applied Computational Intelligence and Soft Computing
Volume 2021, Article ID 8830395, 14 pages
https://doi.org/10.1155/2021/8830395

Research Article

Genetic Algorithms and Particle Swarm Optimization Mechanisms for Through-Silicon Via (TSV) Noise Coupling

Khaoula Ait Belaid,[1] **H. Belahrach**,[1,2] **and H. Ayad**[1]

[1]*Laboratory of Electrical Systems and Telecommunications, Department of Physics, Faculty of Sciences and Technology, Cadi Ayyad University, Marrakesh, Morocco*
[2]*Department of Electrical Engineering, Royal School of Aeronautics, Marrakesh, Morocco*

Correspondence should be addressed to Khaoula Ait Belaid; aitbelaid.khaoula@gmail.com

Received 24 August 2020; Revised 7 January 2021; Accepted 12 May 2021; Published 24 May 2021

Academic Editor: Ridha Ejbali

In this paper, two intelligent methods which are GAs and PSO are used to model noise coupling in a Three-Dimensional Integrated Circuit (3D-IC) based on TSVs. These techniques are rarely used in this type of structure. They allow computing all the elements of the noise model, which helps to estimate the noise transfer function in the frequency and time domain in 3D complicated systems. Noise models include TSVs, active circuits, and substrate, which make them difficult to model and to estimate. Indeed, the proposed approaches based on GA and PSO are robust and powerful. To validate the method, comparisons among the results found by GA, PSO, measurements, and the 3D-TLM method, which presents an analytical technique, are made. According to the obtained simulation and experimental results, it is found that the proposed methods are valid, efficient, precise, and robust.

1. Introduction

The Integrated Circuit (IC) technology evolution is motivated by the need to increase performance in addition to functionality, consequently reducing power and cost. To achieve this objective, several solutions have been used such as scaling devices and associated interconnecting wire by implementing new materials [1, 2] and founding enhancing architecture to reconfigure routing, hierarchy, and building circuits [2, 3]. The integration of different signals and technologies by increasing drive introduces various design concepts for which planar (2D) technologies cannot be suitable. The conventional planar IC has limited establishment choices, and these limit system architecture performance improvements. This causes several problems associated with the interconnection loading in the network of long wires and the need for signal repeaters for clock distribution [2]. Thus, three-dimensional (3D) integrated circuits have been adopted. The 3D technology solves the problems linked to interconnection delays, by reducing the gate delays and increasing interconnections using the short wires. These shorter wires decrease the average load capacitance and resistance and decrease the number of repeaters needed to regenerate the signal on long wires. In addition, to enable integration of heterogeneous technologies, in the 3D design, a 2D chip is divided into several parts, and each one is placed on a separate layer where each layer is stacked on top of each other. This may be exploited to build SoC by placing different circuits with performance requirements in different layers [4, 5].

In 3D technology, the communication between stacked integrated circuits and devices requires vertical interconnections. The processing of vertical interconnections seems complicated compared to the planar one; indeed, having the electrical and mechanical characteristics could be very challenging. Several kinds of vertical interconnection have been proposed such as bonding wires, metal bumps, and contactless communication in addition to Through-Silicon Via (TSV), and a lot of them are popular in the industry. To improve electrical performance, the TSV interconnections

become the first choice to avoid using bonding wires and metal bumps.

The study of 3D architectures requires modeling the TSVs to extract equivalent circuits that describe the electrical characteristics of a specific interconnection structure. In relation to the topic, several papers have discussed the issue of modeling TSVs. In [6, 7], the authors proposed a methodology based on RF characterizations and simulations, leading to a frequency-dependent analytical model including the MOS effect of high-ratio TSV. The authors in [8] gave an efficient method to model TSV interconnections; this approach results in equivalent network parameters that include the combined effect of the conductor, insulator, and silicon substrate. Although the modeling method is based on solving Maxwell's equations in an integral form, the method uses a small number of global modal basis functions and can be much faster than discretization-based and integral equation methods. In [9], an electrical model of TSV which concerns metal-oxide-semiconductor (MOS) capacitance effects was proposed. Design guidelines were proposed for TSVs as variable capacitors. The MOS capacitance was accurately solving Poisson's equation in cylindrical coordinates. Another compact wideband equivalent circuit model for electrical modeling of TSV has been presented in [10]. Rigorous closed-form formulas for TSV inductance and TSV resistance have been derived from the magneto-quasi-static theory with a Fourier–Bessel expansion technique, whereas analytical formulas from static solutions have been used to define the capacitance and conductance. This equivalent circuit model can contain the important parasitic effects of TSVs including the lossy effect of silicon, proximity effect, skin effect, and semiconductor effect. Another different model of TSV in high frequency has been given in [11, 12]. This proposed model includes not only the TSV but also some additional components when using TSVs for 3D-IC, such as the redistribution layer (RDL) and the bump. The model is developed with analytic equations derived from the physical structure. In other previous works [13], the RLC parameters of TSV were modeled as a function of physical parameters and material characteristics. The RLC model is used to predict the inductance, resistance, and capacitance of TSV architectures. Indeed, the TSV impedance can also be extracted using a fully analytical and physical model and Green's function at high frequency [14].

All the previous works have given models of one TSV without considering multi-TSV structures. The modeling of these structures and their time domain simulation is one of the most important problems being studied in this domain. In complicated 3D structures, more signal TSVs are needed, so the TSV distribution density increases. Due to the highly dense distribution of TSVs, TSV noise coupling is expected to be a major concern for 3D-IC system design. Few papers have modeled the noise coupling problem in structures with several TSVs. In [15], the authors have described the equivalent circuit model of the differential TSV pair. The critical differential characteristics are calculated and analyzed based on the lumped circuit model of multi-TSVs. A novel π-type equivalent circuit model of signal-ground TSV pairs which considers proximity effects and eddy current is suggested in [16]. In [17], the authors have presented parasitic substrate coupling effects in 3D-IC due to TSVs. Electrical characterization is performed by dedicating some test structures to extract electrical models of substrate coupling with RF signals. In [12, 18, 19], a TSV noise coupling model is proposed based on a three-dimensional transmission line matrix method (3D-TLM). Using the proposed TSV noise coupling model, the noise coupling transfer functions from TSV to TSV and TSV to the active circuit can be estimated in complicated 3D structures.

The contribution of this work is to propose two intelligent techniques to estimate all elements that composed the models of the noise coupling in 3D structures based on TSVs. The interest of the proposed methods is to prove the potential of artificial intelligence in estimating the elements of microelectronic circuits, since intelligent algorithms are little used in these circuits despite their ability and robustness. The objective of this work is to prove that the proposed approaches based on Genetic Algorithms (GAs) and Particle Swarm Optimization (PSO) can be used with analytical methods in the field of microelectronics.

In this paper, a TSV noise coupling model based on structures studied in [12, 18, 20], GA and PSO, is estimated. This work consists of comparing the parameters found by GA and PSO and those calculated using 3D-TLM and measurements of [12, 18]. By employing GA and PSO, the 3D-substrate parameters can be computed at high frequencies. In additions, the models include most of the elements presented in actual circuits, such as a redistribution layer (RDL) interconnects and substrate contact. The found parameters using GA and those by PSO can be used to estimate the noise coupling in the time domain.

The rest of this paper is organized as follows. In Section 2, first, the noise coupling models in 3D-IC are described; then, GA and PSO are applied to compute the element values of these models. The verification of the results and simulations are given in Section 3. The conclusions are provided in the last section.

2. TSV Noise Coupling Identifications Using Intelligent Methods

2.1. TSV-TSV and TSV-Active Circuit Noise Coupling. Noise coupling in 3D-IC based on TSV is a significant problem which causes serious effects. This type of noise degrades the circuit performance and makes system sensitivity dominated. It can directly be transmitted to an active circuit via the substrate; therefore, the signal and power are corrupted, the system reliability is reduced, and the bit error rate is increased [21, 22]. A TSV is composed of a conductor surrounded by an insulation layer with a very small thickness, which causes an important capacitance between the TSV and the substrate; as a consequence, at high frequencies, a noise can be easily coupled from one TSV to another or substrate and vice versa. In 3D-IC systems, more signal TSVs are used in a limited plane surface as illustrated in Figure 1, which increases the distribution density of TSVs. Because of this greater density, modeling noise coupling between TSVs as well as TSV and active circuits is an

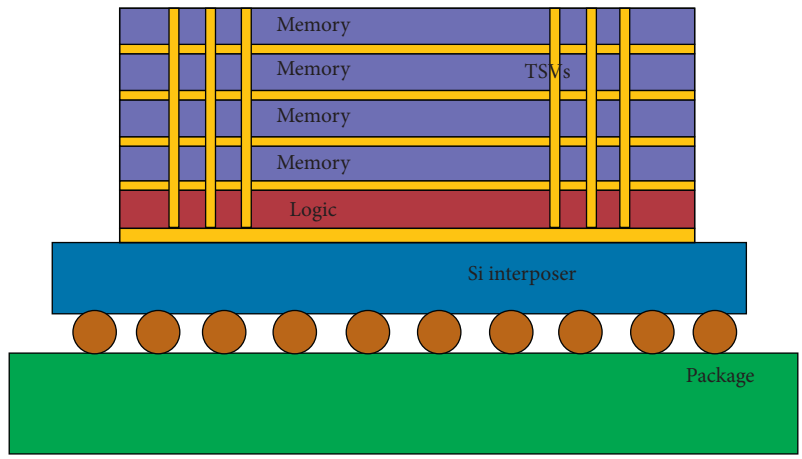

Figure 1: 3D-IC using TSVs.

essential step of the design of these systems [23]. In this section, a TSV noise coupling model is given. The noise can be coupled through many paths: TSV to TSV or TSV to the substrate. For both paths, a model must be given.

The conceptual structure of TSV-to-TSV noise coupling is shown in Figure 2. To model a circuit with several TSVs, a basic structure had been adopted. This structure contains two signal TSVs, where one presents the aggressor and the other the victim, in addition to two ground TSVs connected using a ground line. Figure 3 shows the described structure. The previous structure could be modelled as an equivalent RLGC circuit based on the geometry and material properties. The RLGC circuit consists of a simple TSV's equivalent model, RDL's model, and substrate's model. The TSV model is composed of a capacitance C_{TSV} that represents the insulation layer surrounding the TSV. This capacitance can be derived from the coaxial-cable capacitance model since the TSV is filled with metal and the substrate is conductive, as well as a resistance R_{TSV} representing the material loss and the inductance which considers both the self-inductance $L_{TSV\text{-}self}$ and the mutual inductance $L_{TSV\text{-}mutual}$. The elements of the TSV model are given by the following equations:

$$
\begin{aligned}
C_{TSV} &= \varepsilon_{oxTSV} \times \frac{2\pi h_{TSV}}{\ln\left(r_{TSV} + t_{oxTSV}/r_{TSV}\right)}, \quad [F],\\
R_{TSV} &= \frac{1}{\sigma_{TSV}} \times \sqrt{\left(\frac{h_{TSV}}{\pi r_{TSV}^2}\right)^2 + \left(\frac{h_{\text{sub}}}{\pi\left(r_{TSV}^2 - \left(r_{TSV} - \delta_{SKIN}\right)^2\right)}\right)^2}, \quad [\Omega],\\
\delta_{\text{SKIN,depth}} &= \frac{1}{\sqrt{\pi f \mu \sigma_{TSV}}}, \quad [m],\\
L_{TSV-\text{self}} &= \frac{\mu h_{TSV}}{4\pi} \times \left[\ln\left(\frac{h_{TSV}}{r_{TSV}} + \sqrt{\left(\frac{h_{TSV}}{r_{TSV}}\right)^2 + 1}\right) + \frac{r_{TSV}}{h_{TSV}} - \sqrt{\left(\frac{r_{TSV}}{h_{TSV}}\right)^2 + 1}\right], \quad [H],\\
L_{TSV-\text{mutual}} &= \frac{\mu h_{TSV}}{4\pi} \times \left[\ln\left(\frac{h_{TSV}}{p_{TSV}} + \sqrt{\left(\frac{h_{TSV}}{p_{TSV}}\right)^2 + 1}\right) + \frac{p_{TSV}}{h_{TSV}} - \sqrt{\left(\frac{p_{TSV}}{h_{TSV}}\right)^2 + 1}\right], \quad [H],
\end{aligned}
\tag{1}
$$

where h_{TSV} is the TSV height, r_{TSV} is the TSV radius, t_{oxTSV} is the oxide thickness, p_{TSV} is the pitch between TSVs, σ_{TSV} is the TSV conductivity, ε_{oxTSV} is the oxide permittivity, μ is the magnetic permeability, and δ is the skin depth dependent on material characteristics and on the frequency f.

Because of its distributed nature, the substrate cannot be translated into a compact analytic model accounting the entire chip area whose global effects are felt everywhere in the chip [24, 25]. In most cases, the substrate coupling models can be extracted from full 3D numerical simulations

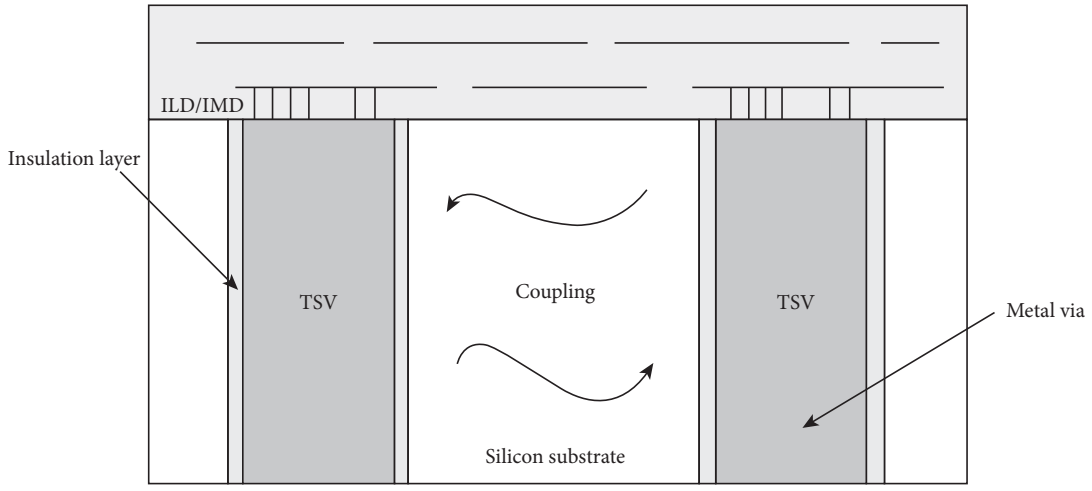

Figure 2: A conceptual view of TSV-TSV noise coupling.

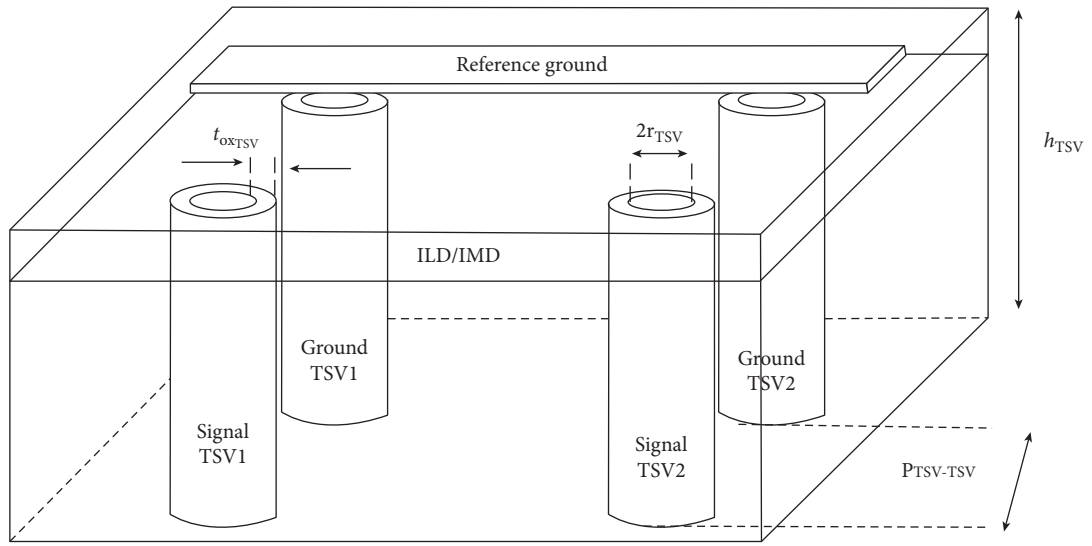

Figure 3: Structure of the TSV-TSV coupling noise.

using lumped-element models or a discretization of a simplified form of Maxwell's equations. The box integration formulation [26, 27] can also help to identify a distributed RC network. In this technique, a 3D rectangular RC mesh network is constructed as an equivalent circuit representation of the modeled substrate. Based on this technique, the equivalent circuit model of the TSV-TSV coupling is given in Figure 4. The equivalent circuit is composed of $C_{TSVtotal}$, which represents the sum of C_{TSV} and C_{RDL}, in addition to five resistances and five capacitances which represent the substrate among the TSVs and L_{gnd} the inductance of the metal connection between ground TSVs. In this equivalent circuit, the inductive coupling is negligible because the bottom side of the TSV is open. The TSV resistance does not influence the TSV-TSV noise coupling and is also neglected in the model.

The lumped circuit in Figure 4 can be simplified into the equivalent circuit model in Figure 5 using the techniques mentioned in [26, 28]. This equivalent circuit contains only three elements: the total equivalent TSV capacitance, substrate resistance, and substrate capacitance. Calculating these parameters is a delicate task; indeed, the authors in [18] used the 3D-TLM method to do so. This technique can be used if a transmission line has a length smaller to the target wavelength. Using the 3D-TLM, the entire TSV coupling test structures are divided into several unit cells of TSV, a silicon substrate, substrate contact, and metal/RDL. Each unit cell is modeled using lumped R, C, L, and G elements, and the entire TSV noise coupling model is then constructed by combining these unit cell models in an appropriate manner. In [18], method parameters as well as the formulas for determining the components of the circuit had been discussed in detail before and after simplification.

Since a 3D-IC contains many silicon chips stacked by TSVs and several MOSs are on these chips [29], the TSV-active circuit coupling must be modeled and analyzed. The conceptual view of this type of noise is depicted in Figure 6. The structure in this figure is difficult to model because it

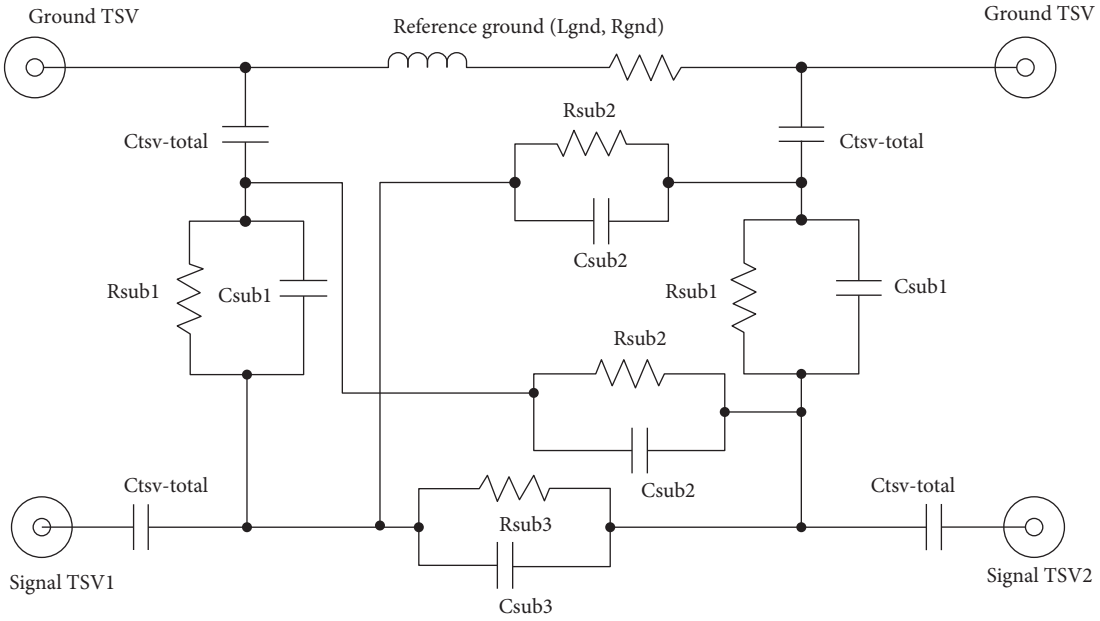

Figure 4: The equivalent circuit model of TSV-TSV noise coupling.

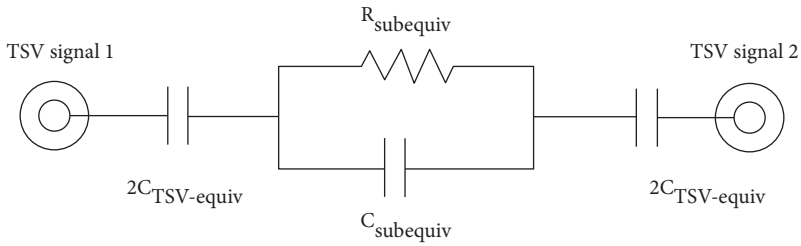

Figure 5: A simplified model of the TSV-TSV noise coupling circuit.

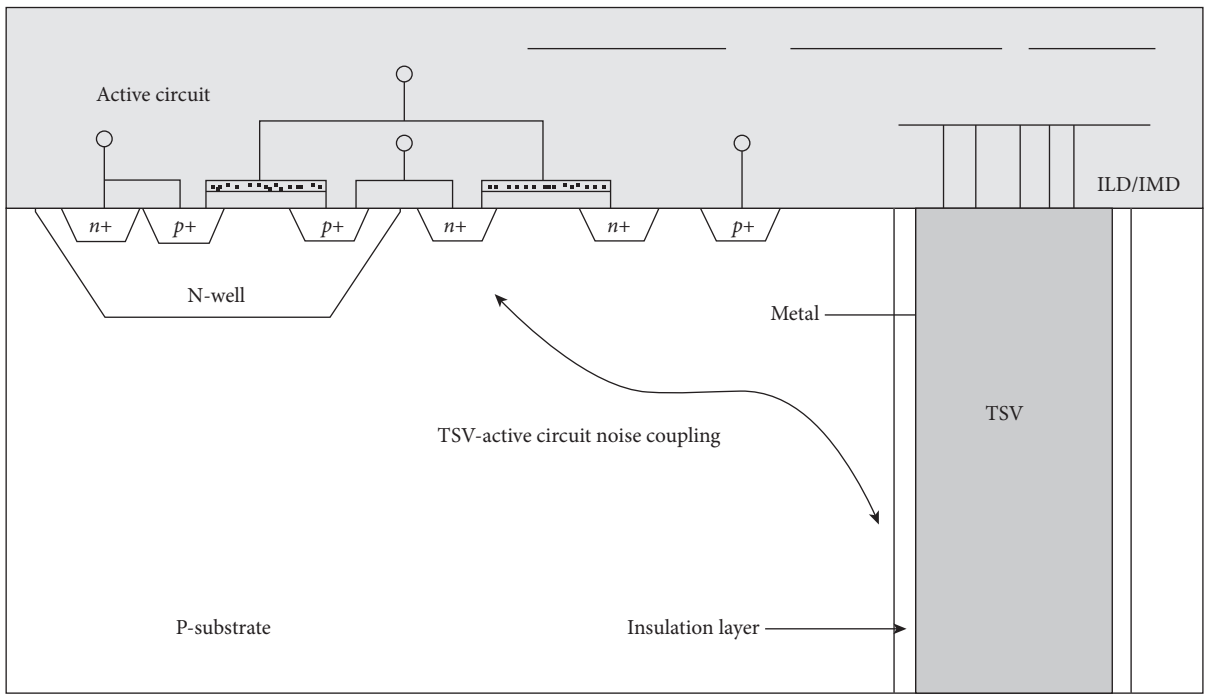

Figure 6: The conceptual view of TSV-active circuit noise coupling.

includes many active circuits. Therefore, a simplification that considers a substrate contact instead of an active circuit was used. The P^+ contact in a p-type silicon substrate can be represented as an active circuit, and the noise coupling between the TSV and the contact can be represented as the coupling between the active circuit and the TSV [18].

The test structure and physical parameters of TSV-contact noise coupling are presented in Figure 7. The equivalent circuit model representing this structure is illustrated in Figure 8. Similar to the equivalent circuit of TSV-TSV noise coupling, the model is composed of $C_{TSVtoal}$, which is the sum of C_{TSV} and C_{RDL} and R_{sub} and C_{sub}, in addition to C_{ref} and L_{gnd} which represent the ground-line parameters. The lumped circuit model in Figure 8 can be simplified into the total equivalent circuit model in Figure 9, which contains only three elements: the total equivalent TSV capacitance ($C_{TSV\text{-}equiv}$), the substrate resistance ($R_{sub\text{-}equiv}$), and the substrate capacitance ($C_{sub\text{-}equiv}$). In the case of the TSV-active circuit, it is difficult to propose equations to compute the substrate resistance and capacitance values. Therefore, the authors in [18] used the 3D-LTM technique as explained before, and in this work, genetic algorithms were adopted to optimally search these values.

The objective of this study was to calculate the parameters of the simplified circuit presented in Figures 5 and 9, using intelligent methods GA and PSO.

2.2. Intelligent GA. Genetic algorithms are based on natural selection. They are a technique for solving optimization and control problems. These algorithms are based on the repeated modification of the population to arrive at an optimal solution [30–33]. To create new individuals (solutions) from the current population at each generation, genetic algorithms use three main rules: selection, crossover, and mutation. Genetic algorithms are controlled by a fitness function which measures the performance of each individual. The diagram in Figure 10 summarizes the principle and the main steps of GA optimization.

Genetic algorithms differ from classical optimization in four points: the solution is found from a set of points and not from a single point, the regularity of the studied function is not imposed, they are not determinist and use probabilistic transition rules, and no hypotheses of linearity or normality are used.

2.3. Intelligent PSO. Particle swarm optimization (PSO) was developed by Kennedy in 1995 for difficult optimization problems. The principle of PSO was inspired by the social behavior of animals moving such as bird flocking. When the movement aims to find food, each bird flies in the space of solutions and specifies its speed according to its experience and the information obtained by other swarm individuals [34].

The principle of PSO begins with an initialization matrix which contains N particles scattered in the exploration space along dimension j for $j = \{1, 2, \ldots, D\}$. Each individual P_i ($i = 1, 2, \ldots, N$) keeps its best position $Bp_i(t+1)$ and the best solution of its proximity B_{pp} $(t+1)$. The best solution is defined by the position of the particle with the smallest fitness value [35, 36]. The movement of each particle is controlled by three rules. First of all, the particle must follow its actual speed direction. Then, it moves to its best position. Then, it moves to the best position found by its neighbors. Indeed, the new speed matrix V_{ij} and position matrix X_{ij} of particles are computed at $(t+1)$, using the following equations:

$$Bp_i(t+1) = \begin{cases} X_i(t+1), & \text{if } f\left(X_i(t+1)\right) < f\left(Bp_i(t)\right), \\ Pb_i(t), & \text{else,} \end{cases} \tag{2}$$

$$B_{pp} = \min_{i=1,2,\ldots,N} f\left(Bp_i(t)\right), \tag{3}$$

$$\begin{aligned} V_{ij}(t+1) = {} & \omega.V_{ij}(t) + R_{11}C_{11} \otimes \left(Bp_{ij}(t) - X_{ij}(t)\right) \\ & + R_{21}C_{21} \otimes \left(Bpp_{ij}(t) - X_{ij}(t)\right), \end{aligned} \tag{4}$$

$$X_{ij}(t+1) = X_{ij}(t) + V_{ij}(t+1), \tag{5}$$

where Bp_{ij} is the best position found by the particle *i;* Bpp_{ij} is the best position found by the neighbors; ω, C_{11}, and C_{21} are the weighting coefficients; and R_{11} and R_{21} are the random variables generated from a uniform distribution in [0, 1].

2.4. Identification Strategy. Our objective was to identify the parameters of the equivalent model of the TSV-TSV coupling as well as the TSV-active circuit coupling based on GAs, PSO, and the experimental measurements of [12, 18]. The steps to follow in our technique are presented in Figure 11.

To perform this task, the following steps were carried out: first of all, the curve of experimental measurements which must be followed by the theory was drawn, then the transfer function of the circuit according to unknown parameters, $C_{TSV\text{-}equiv}$, $R_{sub\text{-}equiv}$, and $C_{sub\text{-}equiv}$, was calculated, and finally, GAs tried to find these parameters by making several iterations until the two curves were pasted together; the objective is to minimize the error between the experimental curve and the transfer function of the TSV noise coupling model. For genetic algorithms to work properly, mutation, crossover, selection, and fitness function parameters all must be chosen correctly.

The same strategy was followed for PSO to optimally estimate the coupling noise parameters. Therefore, its parameter setting must also be chosen correctly.

In our problem for both intelligent algorithms, the fitness function was defined as the square of the difference between the experimental curve and the theoretically calculated transfer function or the square error. In fact, GAs and PSO optimized requested parameters by minimizing this error and made it to zero.

For TSV-active circuit noise coupling, Genetic Algorithms had been used as explained for the first, just that the transfer function and the experimental curve changed.

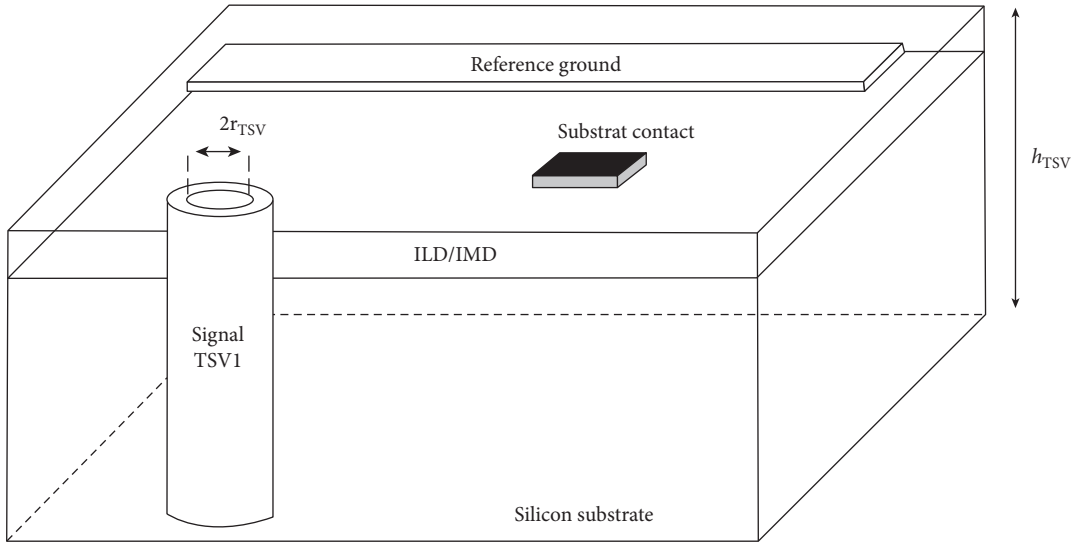

Figure 7: Structure of the TSV-active circuit noise coupling.

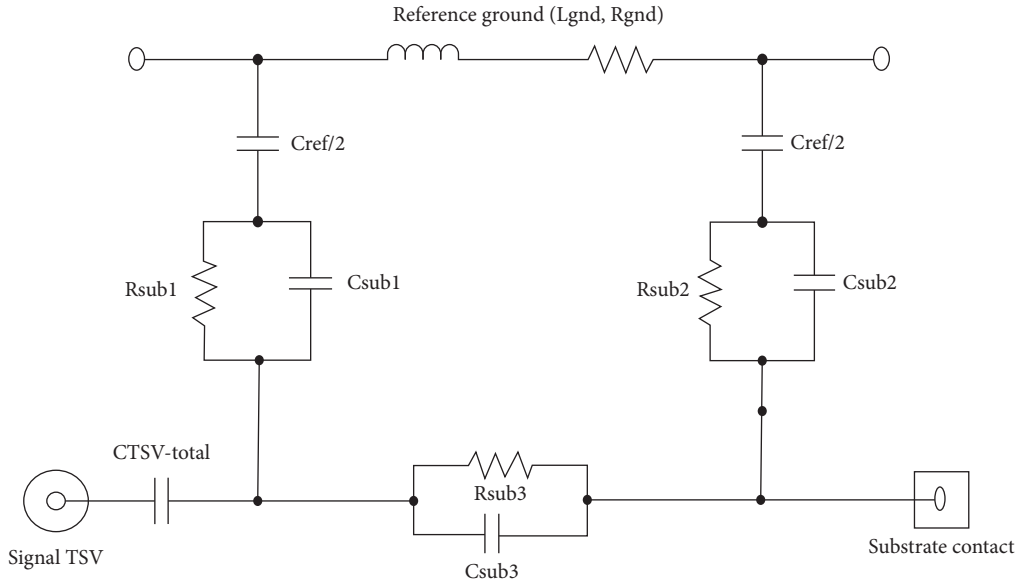

Figure 8: The equivalent circuit model of TSV-active circuit noise coupling.

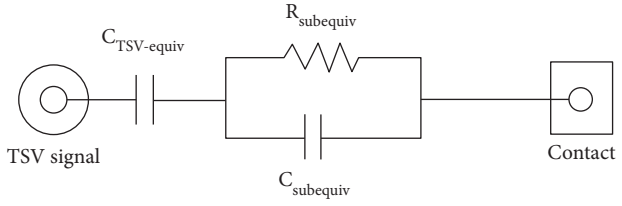

Figure 9: A simplified model of the TSV-active circuit noise coupling circuit.

3. Results and Discussion

In this section, the proposed methods GA and PSO are verified by frequency- and time-domain measurements published in [12, 18]. So, all measurement curves used in this work were taken from these last references. To take the measurements of TSV-TSV noise coupling and verify its model, the test vehicles in Figures 3 and 7 were fabricated using the Hynix via-last TSV process; according to this process, the RDL effects are significant, cannot be neglected, and presented by C_{RDL} added to C_{TSV}. Concerning the manufacturing process of TSV, the top of the TSV was caved in, which prevents direct probing on the TSV, and the RDL line was used for the probing pad. The TSV had no interconnection on the bottom side, and the vehicle was placed on an insulator to isolate the conductive silicon substrate from the environment. The effects of the insulator were neglected because of its low dielectric constant [12, 18]. An analyzer (VNA) was used to take measurements from 10 MHz to 20 GHz. Table 1 shows all physical dimensions and material properties of the test vehicle.

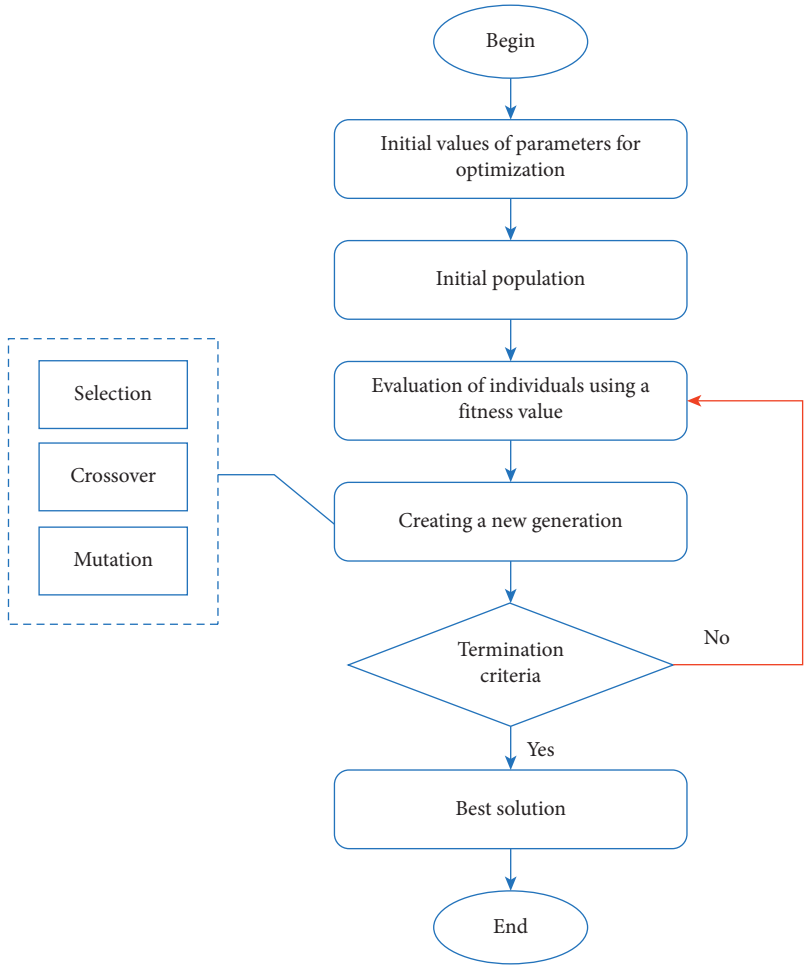

Figure 10: The principal of genetic algorithms.

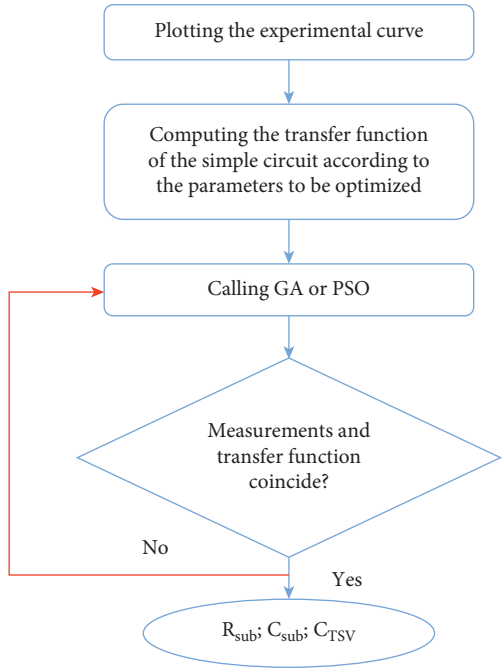

Figure 11: Identification strategy.

For adjusting GA and PSO, which were used to calculate the circuit parameters presented by Figures 5 and 9 in such a way that the circuit transfer function that depends on these parameters follows the measurements whether in the frequency domain or the time domain, the parameters mentioned below were used. These parameters had been chosen carefully to ensure that the intelligent GA and PSO are effective.

For GA, the population size of each generation was fixed at 100 individuals. The individuals of the algorithm are the parameters to find. The mutation was Gaussian. Two-point crossover with a crossover probability of 0.5 was used. The idea behind the multipoint crossover is that parts of the chromosome that contribute to the fit behavior of an individual may not be in adjacent substrings. Furthermore, the disruptive nature of multipoint crossover may result in a more robust search by encouraging exploration of the search space rather than early convergence to highly fit individuals [37]. The tournament selection with a tournament size of 10 was used to select the parents at each generation. In tournament selection, the individuals are chosen randomly from the generation and the best individual from this part is chosen as a parent. This is repeated until enough parents have been chosen to produce the required number of individuals for the next generation.

Table 1: Physical dimensions and material properties of the test vehicle.

Component	Value (μm)	Component	Value	Component	Value (μm)
r_{TSV}	16.5	σ_{sub}	10 S/m	$d_{\text{TSV-TSV}}$	130
t_{oxTSV}	0.52	σ_{TSV}	5.8×10^7 S/m	$p_{\text{TSV-TSV}}$	250
h_{sub}	100	$\varepsilon_{r,\text{sub}}$	11.9		

For PSO, $N = 500$, indeed the exploration space contains all possible solutions, D is set to 3. The compromise between local and global exploration is ensured by $\omega = 0.7$, $C_{11} = 0.8$ to avoid the problem of fast convergence, and $C_{21} = 1.2$ to enhance the global best solution. The maximum number of generations is set to 30.

The fitness function, for both intelligent algorithms, was the square of the error (the difference) between experimental measurements and the fitness function of the circuit. The simulations performed in this work were realized using Matlab tool. Comparisons with the results presented in [12–14, 18], which use the 3D-TLM analytical method to calculate the parameters to be found, have been made.

The parameters found by GAs, PSO, and 3D-TLM of [12, 18] are given in Table 2. The measured noise and the noise transfer function of TSV-TSV coupling, in the frequency domain, using GA's parameters and PSO's parameters, in addition to the noise transfer function with the parameters in [12, 18], are illustrated in Figure 12. The noise transfer function was calculated when both ports are terminated with 50 Ω resistances.

Based on the results reported in Figure 12, the proposed methods, measurements, and 3D-TLM agree well despite the difference which appeared in the frequencies higher than 3 GHz. Therefore, the method verification based on the measurement is valid. By analyzing the element values of Table 2, one can see that the values calculated by GAs and PSO are close to those given by 3D-TLM. Yet, GAs and PSO generate a curve closer to that of measurements at high frequencies. The difference between the curves can be explained by the fact that the models estimate the low noise transfer function at high frequencies, where even low capacities cannot be neglected, or by a change in the characteristics of the test vehicle or by measurement errors.

Figure 12 shows that GA and PSO perform the identification of all models' parameters with high precision. The model's response with GA and PSO are very close to the experimental measurements. These observations prove the efficiency of GA and PSO to find good solutions, even if identifying is a hard task.

Observing Figure 12, the TSV-TSV noise coupling is divided into 3 regions. In region 1, from 10 MHz to 1 GHz, the $C_{\text{TSV-equivalent}}$ is the principal contributing element since the equivalent TSV is larger than the equivalent substrate resistance. In region 2, from 1 GHz to 12 GHz, the noise transfer function is defined by $R_{\text{sub-equiv}}$ because it becomes larger than $_{\text{CTSV-equiv}}$ impedance and smaller than $C_{\text{sub-equiv}}$ impedance. In region 3, frequencies are above 12 GHz and $R_{\text{sub-equiv}}$ is larger than $C_{\text{TSV-equiv}}$ impedance and $C_{\text{sub-equiv}}$ impedance, so the noise transfer function is given by $C_{\text{sub-equiv}}$. The more the frequency increases, the more the noise increases.

Table 2: TSV-TSV noise coupling parameters using GA and 3D-TLM.

Methods	$C_{\text{TSV-equiv}}$ (fF)	$R_{\text{sub-equiv}}$ (Ω)	$C_{\text{sub-equiv}}$ (fF)
GAs	192.375	835.13	16.94
PSO	197.12	840.46	15.72
3D-TLM	201.3	928.5	11.2

The proposed methods in this work must also respect the transfer function in the time domain. Indeed, if the GA and PSO find parameters that correspond to the transfer function in the frequency domain, but do not go to with the time domain, the tests must be redone. Since the values found by the two intelligent algorithms are close, the test in the time domain is plotted just for GAs. The proposed and measurement method of the TSV-TSV noise coupling of the test vehicle in the time domain at frequencies 100 MHz and 1 GHz is illustrated, respectively, in Figures 13 and 14. For temporal simulations, a trapezoidal signal switching from 0 to 1 V with a rising/falling time of 40 ps and source resistance of 50 Ω was used on port 1 and the coupling noise on port 2 was simulated using PSPICE tool. According to Figures 13 and 14, the method used to compute the parameters of Figure 5 is verified and valid. Indeed, the proposed method can be adopted for the calculation of coupling noise parameters in a 3D structure based on TSVs. Based on Figures 13 and 14, we can also notice that the coupling is important and exceeds 80 mV in 3D structures based on TSVs.

For the TSV-active circuit coupling model, by using GA and PSO, each lumped circuit value in Figure 9 was obtained. The population size of each GA's generation was fixed at 100 individuals. The mutation was defined as 0.2, 2-point crossover with a crossover probability of 0.4 was used, and the tournament selection with a tournament size of 10 was chosen. For PSO, $N = 1000$, D is set to 3, $\omega = 0.7$, $C_{11} = 0.8$, and $C_{21} = 1.2$, and the maximum number of generations is set to 15. The fitness function is the square of the difference between experimental measurements and the transfer function of the circuit. The element values of the lumped circuit of TSV-contact coupling computed by the proposed methods and 3D-TLM are presented in Table 3.

The measured, the 3D-TLM method, and the proposed methods for the TSV-contact coupling noise are illustrated in Figure 15. Based on the results presented in this figure, the proposed methods closely matched the experimental results and 3D-TLM method. The proposed methods' verification based on the measurements was valid. GAs and PSO were more efficient than the 3D-TLM method since the curves

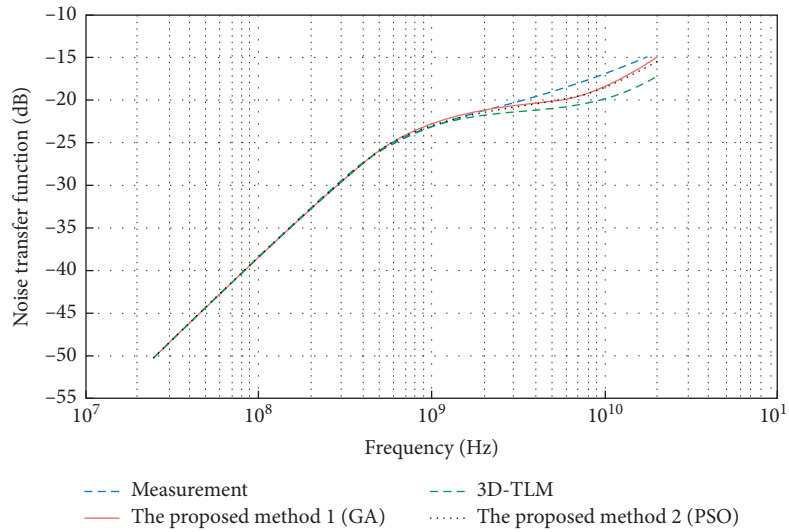

Figure 12: The proposed method, measured, and 3D-TLM noise transfer function of TSV-TSV noise coupling.

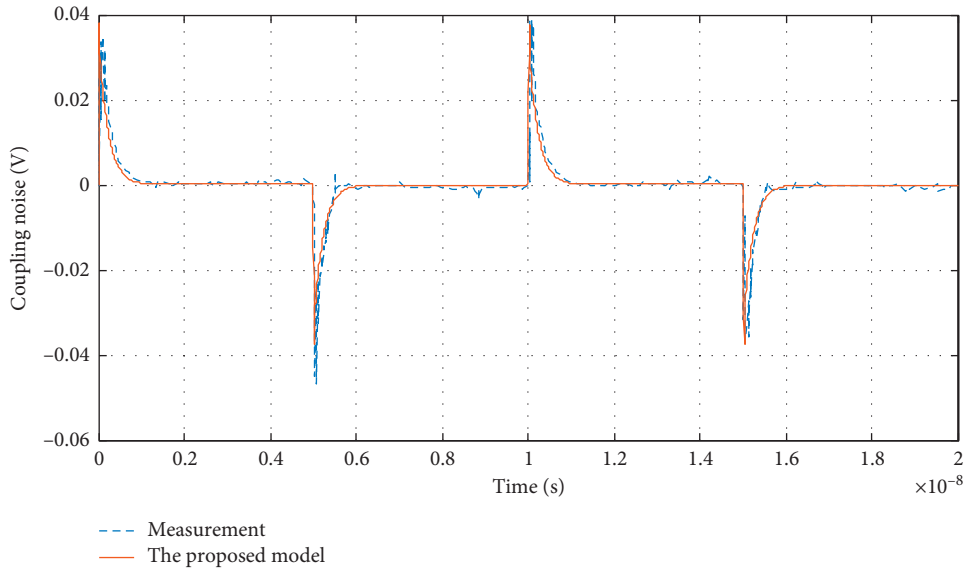

Figure 13: The proposed method and measured TSV-TSV coupling noise in the time domain (the input clock frequency at port 1 is 100 MHz).

given by these intelligent algorithms are closer to the measurements than that given by the 3D-TLM technique.

The TSV-contact noise coupling is identical to the TSV-TSV noise coupling. The transfer function is divided into three frequency behaviors regions, where each region was dominated by an element of the model in Figure 9 as already explained above. In this case, as the frequency increases, the noise increases; in addition, the noise is more important than the TSV-TSV case; this is due to the high value of $C_{TSV\text{-}equiv}$ of a single TSV.

The simulations in the time domain for the GA method are presented in Figures 16 and 17, respectively. These simulations were performed using the same characteristics cited for TSV-TSV noise. A trapezoidal signal switching from 0 to 1 V with a rising/falling time of 40 ps and source resistance of 50 Ω was used. The simulations were made in the PSPICE tool at 100 MHz and 1 GHz.

By analyzing the results of Figures 16 and 17, one can see that the proposed method gave a behavior that reflects the experimental. Therefore, the proposed method was validated in the time domain as well as the frequency domain.

Observing Figures 13, 14, 16, and 17, the peak-to-peak noise coupling in both studied cases is about 0.08 V. This value is already high and can even increase; therefore, these noises should be considered.

Modeling 3D structures based on TSVs seems to be a very complicated task that needs to be taken into consideration. Many well-known analytical methods such as FDTD and 3D-TLM had been used to achieve this objective. These methods require a lot of calculation and time, but they are

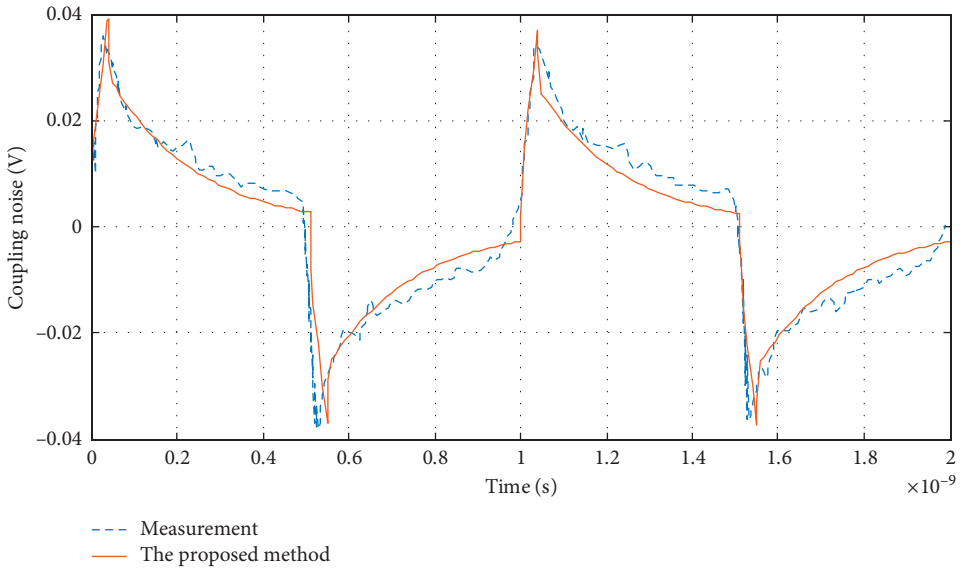

Figure 14: The proposed method and measured TSV-TSV coupling noise in the time domain (the input clock frequency at port 1 is 1 GHz).

Table 3: The TSV-contact noise coupling parameters using GA and 3D-TLM.

Methods	$C_{TSV\text{-}equiv}$ (fF)	$R_{sub\text{-}equiv}$ (Ω)	$C_{sub\text{-}equiv}$ (fF)
GAs	815.21	870.74	14.08
PSO	808.13	880.13	13.93
3D-TLM	817.5	879.8	12

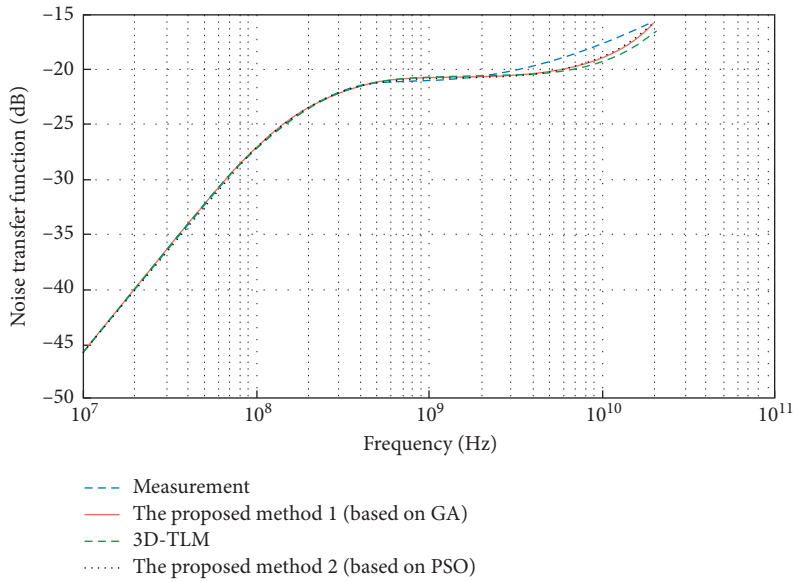

Figure 15: The proposed method, measured, and 3D-TLM noise transfer function of TSV-contact coupling.

suitable. This work had adopted two intelligent methods (GA and PSO) that are rarely used in this field.

The results found in this work, based on GA and PSO, were conventional to experimental results. These results were even closer than those found by 3D-TLM used in [18]. It is true that both methods found similar results, but a small improvement validated by the experimental was noticed by the proposed methods. The results proved that intelligent methods are effective and robust.

In this work, a complicated model with several TSVs (more than two) was presented; this model was replaced by another reduced model, which is similar to the coupling model between two TSVs but reflects the coupling behavior of several TSVs. From the found results, it can be concluded

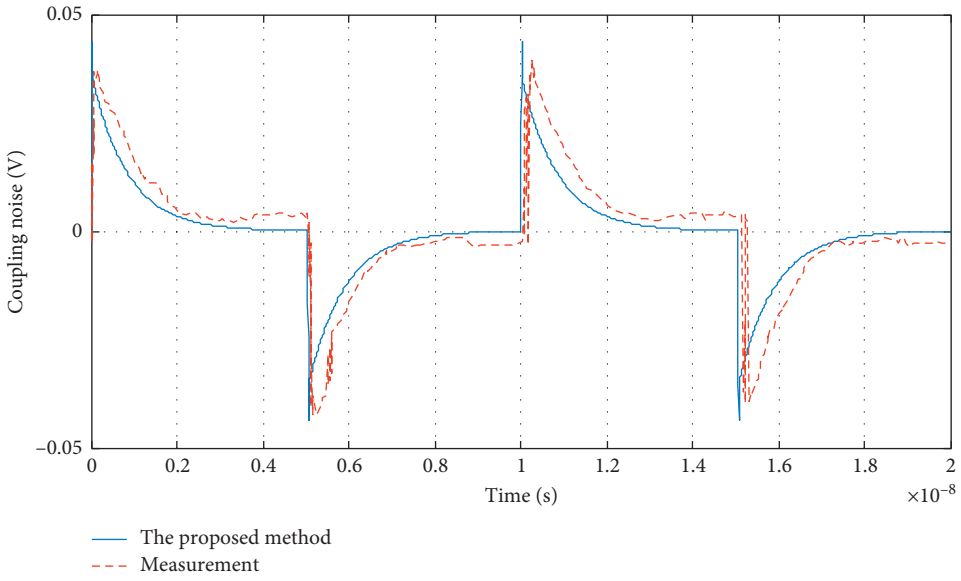

Figure 16: The proposed method and measured coupling noise of TSV-contact in the time domain (the input clock frequency at port 1 is 100 MHz).

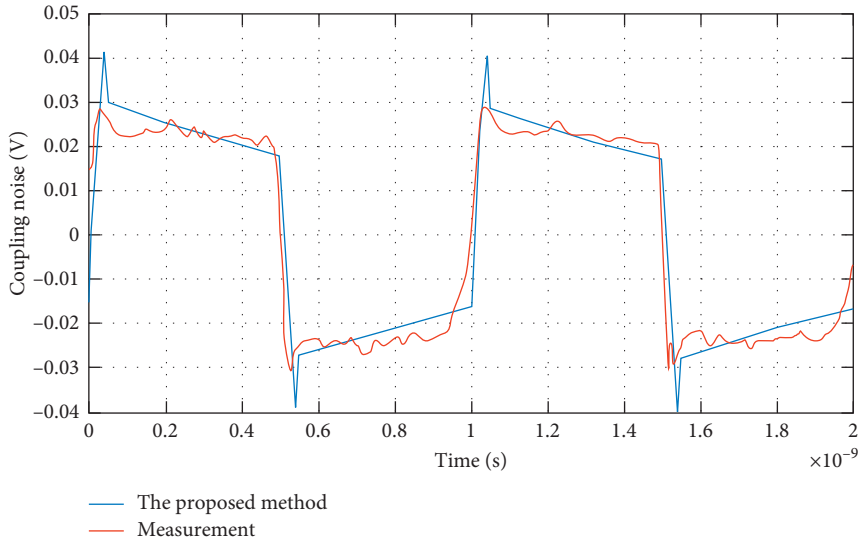

Figure 17: The proposed method and measured coupling noise of TSV-contact in the time domain (the input clock frequency at port 1 is 1 Ghz).

that any structure with several TSVs in the same level can be replaced by the simple model, it is just necessary to find a method to compute the parameters of the reduced circuit, and as already explained, GAs and PSO remain a good tool.

4. Conclusions

3D integrated architectures based on TSVs are a relatively new research and widely used. Yet, these architectures have some difficulties mainly in their modeling and analysis. Accordingly, new methods to model them are necessary.

In this paper, intelligent methods based on genetic algorithms (GAs) and recent heuristic optimization of particle swarm optimization (PSO) were proposed to identify the parameters of TSV-TSV and TSV-contact noise coupling in 3-D IC design. Both models included the equivalent circuit of the TSV, RDL, metal interconnects, and the substrate. Indeed, the model can represent a practical 3D-IC system design. Using GA and PSO, the parameters of previous models were found which substantiated to estimate the noise transfer function in three frequency regions from 10 MHz to 20 GHz.

To validate the proposed techniques based on GAs and PSO, frequency and time measurements as well as the analytical method used in [18] were applied. Obtained results showed a good agreement between the proposed methods

and experiments. They also showed an improvement compared to 3D-TLM. These algorithms were easy to apply, did not require a lot of simulation time, efficient, and robust.

Data Availability

No data were used to support this study.

Conflicts of Interest

The authors declare that they have no conflicts of interest.

References

[1] V. Agarwal, M. S. Hrishikesh, S. W. Keckler, and D. Burger, "Clock rate versus IPC," *ACM SIGARCH Computer Architecture News*, vol. 28, no. 2, pp. 248–259, 2000.

[2] A. W. Topol, D. C. Tulipe, L. Shi Jr et al., "Three-dimensional integrated circuits," *IBM Journal of Research and Development*, vol. 50, no. 415, 2006.

[3] K. Salah, A. El Rouby, H. Ragai, and Y. Ismail, "3D/TSV enabling technologies for SOC/NOC: modeling and design challenges," in *Proceedings of the 2010 22nd International Conference on Microelectronics*, Cairo, Egypt, December 2010.

[4] K. Siozios, A. Bartzas, and D. Soudris, "Architecture-level exploration of alternative interconnection schemes targeting 3D FPGAs: a software-supported methodology," *International Journal of Reconfigurable Computing*, vol. 2008, Article ID 764942, 18 pages, 2008.

[5] D. H. Kim, S. Mukhopadhyay, and S. K. Lim, "TSV aware interconnect length and power prediction for 3D stacked ICs," in *Proceedings of the 2009 IEEE International Interconnect Technology Conference*, pp. 26–28, Sapporo, Japan, June 2009.

[6] L. Cadix, C. Fuchs, M. Rousseau, H. Leduc, and H. Chaabouni, "Integration and frequency dependent parametric modeling of through Silicon via involved in high density 3D chip stacking," *ECS Transactions*, vol. 33, no. 12, pp. 1–21, 2010.

[7] C. Ryu, J. Lee, H. Lee, H. Lee, T. Oh, and J. Kim, "High frequency electrical model of through wafer via for 3D stacked chip packaging," in *Proceedings of the 2006 1st Electronic Systemintegration Technology Conference*, pp. 215–220, Dresden, Germany, September 2006.

[8] K. J. Han, M. Swaminathan, and T. Bandyopadhyay, "Electromagnetic modeling of TSV interconnections using cylindrical modal basis function," *IEEE Transactions on Advanced Packaging*, vol. 33, no. 4, 2010.

[9] T. Bandyopadhyay, K. J. Han, D. Chung, R. Chatterjee, M. Swaminathan, and M. Tummala, "Rigorous electrical modeling of TSVs with MOS capacitance effects," *IEEE Transactions on Components, Packaging and Manufacturing Technology*, vol. 1, no. 6, 2011.

[10] E. X. Liu, E. P. Li, W. B. Ewe, H. M. Lee, and S. Gao, "Compact wideband equivalent circuit model for electrical modeling of TSV," *IEEE Transactions on Microwave Theory and Techniques*, vol. 59, no. 6, 2011.

[11] J. Kim, J. S. Pak, J. Cho et al., "High-frequency scalable electrical model and analysis of TSV," *IEEE Transaction Components Packaging and Manufacturing Technology*, vol. 1, no. 2, pp. 181–195, 2011.

[12] M. Lee, J. S. Pak, and J. Kim, *Electrical Design of through Silicon via*, Springer Dordrecht Heidelberg, London, UK, 2014.

[13] G. Katti, M. Stucchi, K. De Meyer, and W. Dehaene, "Electrical modeling and characterization of through silicon via for three-dimensional ICs," *IEEE Transactions on Electron Devices*, vol. 57, no. 1, pp. 256–262, 2010.

[14] C. Xu, V. Kourkoulos, R. Suaya, and K. Banerjee, "A fully analytical model for the series impedance of through-silicon vias with consideration of substrate effects and coupling with horizontal interconnects," *IEEE Transactions on Electron Devices*, vol. 58, no. 10, pp. 3529–3540, 2011.

[15] C. Qu, R. Ding, and Z. Zhu, "High-frequency electrical modeling and characterization of differential TSVs for 3-D integration applications," *IEEE Microwave and Wireless Components Letters*, vol. 27, no. 8, pp. 721–723, 2017.

[16] Q. Lu, Z. Zhu, Y. Yang, R. Ding, and Y. Li, "High-frequency electrical model of through-silicon vias for 3-D integrated circuits considering eddy current and proximity effects," *IEEE Transactions on Components, Packaging and Manufacturing Technology*, vol. 7, no. 12, pp. 2036–2044, 2017.

[17] E. Eid, T. Lacrevaz, C. Bermond et al., "Characterization and modeling of RF substrate coupling effects in 3D integrated circuit stacking," *Microelectronic Engineering*, vol. 88, no. 5, pp. 729–733, 2011.

[18] J. Cho, E. Song, K. Yoon et al., "Modeling and analysis of through-silicon via (TSV) noise coupling and suppression using a guard ring," *IEEE Transactions on Components, Packaging and Manufacturing Technology*, vol. 1, no. 2, pp. 220–233, 2011.

[19] J. Lim, J. Cho, D. H. Jung et al., "Modeling and analysis of TSV noise coupling effects on RF LC-VCO and shielding structures in 3D IC," *IEEE Transactions on Electromagnetic Compatibility*, vol. 60, no. 6, pp. 1939–1947, 2018.

[20] K. Ait Belaid, H. Belahrach, and H. Ayad, "Numerical laplace inversion method for through-silicon via (TSV) noise coupling in 3D-IC design," *Electronics*, vol. 8, no. 9, 1010 pages, 2019.

[21] Y. Shim, J. Park, J. Kim et al., "Modeling and analysis of simultaneous switching noise coupling for a CMOS negative-feedback operational amplifier in system-in-package," *IEEE Transactions on Electromagnetic Compatibility*, vol. 51, no. 3, pp. 763–773, 2009.

[22] K. Koo, Y. Shim, C. Yoon et al., "Modeling and analysis of power supply noise imbalance on ultra high frequency differential low noise amplifiers in a system-in-package," *IEEE Transactions on Advanced Packaging*, vol. 33, no. 3, pp. 602–616, 2010.

[23] K. Han, "Electromagnetic modeling of interconnections in three-dimensional integration," Dissertation, School of Electrical and Computer Engineering Georgia Institute of Technology, Atlanta, Georgia, 2009.

[24] A. Afzali-Kusha, M. Nagata, N. K. Verghese, and D. J. Allstot, "Substrate noise coupling in SoC design: modeling, avoidance, and validation," *Proceedings of the IEEE*, vol. 94, no. 12, pp. 2109–2138, 2006.

[25] M. Nagata, T. Morie, and A. Iwata, "Modeling substrate noise generation in CMOS digital integrated circuits," in *Proceedings of the IEEE 2002 Custom Integrated Circuits Conference*, pp. 501–504, Orlando, FL, USA, May 2002.

[26] K. J. Kerns, I. L. Wemple, and A. T. Yang, "Stable and efficient reduction of substrate model networks using congruence transforms," in *Proceedings of IEEE International Conference on Computer Aided Design (ICCAD)*, pp. 207–214, San Jose, CA, USA, November 1995.

[27] N. K. Verghese, D. J. Allstot, and S. Masui, "Rapid simulation of substrate coupling effects in mixed-mode ICs," in

Proceedings of IEEE Custom Integrated Circuits Conference-CICC '93, San Diego, CA, USA, May 1993.

[28] D. J. Van Genderen and N. P. Van der Meijs, "Reduced RC models for IC interconnections with coupling capacitances," in *Proceedings of the 1992 European Conference on Design Automation*, pp. 132–136, Brussels, Belgium, March 1992.

[29] P. Nordin, R. E. Keller, and W. Banzhaf, *Genetic Programming: An Introduction: On The Automatic Evolution Of Computer Programs And Its Applications*, pp. 1236–1239, Morgan Kaufmann, Burlington, MA, USA, 1998.

[30] D. Goldberg, *Genetic Algorithms in Search Optimization and Machine Learning*, vol. 412, pp. 95–99, Addison-Wesley, Boston, MA, USA, 1989.

[31] P. Reed, B. Minsker, and D. E. Goldberg, "Designing a Competent simple genetic algorithm for search and optimization," *Water Resources Research*, vol. 36, no. 12, pp. 3757–3761, 2000.

[32] E. Nicoara, "Solving scheduling in pharmaceutical industry with genetic algorithms," *Journal of Control Engineering and Applied Informatics*, vol. 9, pp. 19–26, 2007.

[33] L. Baghli, *Contribution à la commande de la machine asynchrone, utilisation de la logique floue, des réseaux de neurones et des algorithmes génétiques*, Point Carré University, Nancy, France, 1999.

[34] R. Pupeikis, "On recursive parametric identification of wiener systems," *Information Technology and Control*, vol. 40, no. 1, pp. 21–28, 2009.

[35] J. Kennedy and R. C. Eberhat, "Particle swarm optimization," in *Proceedings of ICNN'95-International Conference on Neural Networks*, Perth, Australia, November 1995.

[36] F. Marini and B. Walczak, "Particle swarm optimization (PSO). A tutorial," *Chemometrics and Intelligent Laboratory Systems*, vol. 149, pp. 153–165, 2015.

[37] F. Picarougne, "Recherche d'information sur internet par algorithmes évolutionnaires," Doctoral Thesis, Tours University, Tours, France, 2000.